Published in final edited form as:
*J Med Chem*. 2013 February 14; 56(3): 895–901. doi:10.1021/jm301740k.

# Development of $^{18}$F-Labeled Picolinamide Probes for PET Imaging of Malignant Melanoma

**Hongguang Liu**[1,2,‡], **Shuanglong Liu**[1,‡], **Zheng Miao**[1], **Zixin Deng**[2], **Baozhong Shen**[3], **Xuechuan Hong**[2], and **Zhen Cheng**[1,*]

[1]Molecular Imaging Program at Stanford (MIPS), Bio-X Program, Department of Radiology, Stanford University, California, 94305-5344

[2]Key Laboratory of Combinatorial Biosynthesis and Drug Discovery (Wuhan University), Ministry of Education, Wuhan University School of Pharmaceutical Sciences, Wuhan 430071, PR China

[3]Department of Radiology, Fourth Affiliated Hospital of Harbin Medical University, Harbin, China, 150001

## Abstract

Melanoma is an aggressive skin cancer with worldwide increasing incidence. Development of positron emission tomography (PET) probes for early detection of melanoma is critical for improving the survival rate of melanoma patients. In this research, $^{18}$F-picolinamides based PET probes were prepared by direct radiofluorination of the bromopicolinamide precursors using no-carrier-added $^{18}$F-fluoride. The resulting probes, $^{18}$F-1, $^{18}$F-2 and $^{18}$F-3 were then evaluated *in vivo* by small animal PET imaging and biodistribution studies in C57BL/6 mice bearing B16F10 murine melanoma tumors. Noninvasive small animal PET studies demonstrated excellent tumor imaging contrasts for all probes, while $^{18}$F-2 showed higher tumor to muscle ratios than $^{18}$F-1 and $^{18}$F-3. Furthermore, $^{18}$F-2 demonstrated good *in vivo* stability as evidenced by the low bone uptake in biodistribution studies. Collectively, these findings suggest $^{18}$F-2 as a highly promising PET probe for translation into clinical detection of melanoma.

### Keywords

melanoma; PET; Benzamide

## Introduction

Malignant melanoma is one of the most aggressive and lethal cancers that has increasing incidence world widely, especially in the Caucasian population.[1–2] Its strong tendency to metastasize and absence of effective treatment for advanced diseases result in a poor overall survival.[3–4] Therefore, development of novel and accurate molecular imaging techniques to detect melanoma at its earliest stages is critical for improving the survival of patients that have malignant melanoma.

*Correspondence should be sent to: Zhen Cheng, Ph.D., Molecular Imaging Program at Stanford, Canary Center at Stanford for Cancer Early Detection, Department of Radiology and Bio-X Program, 1201 Welch Road, Lucas Expansion, P095, Stanford University, Stanford CA 94305, 650-723-7866 (V), 650-736-7925(Fax), zcheng@stanford.edu.
‡These authors contributed equally. The manuscript was written through contributions of all authors. All authors have given approval to the final version of the manuscript.

The authors declare no competing financial interest.

Supporting Information Available: RP-HPLC and mass spectrometry data of synthesized compounds. This material is available free of charge via the Internet at http://pubs.acs.org

Over the last a few decades, noninvasive molecular imaging of malignant melanoma with various modalities has been extensively studied; these modalities include radionuclide imaging with positron emission tomography (PET) and single photon emission computed tomography (SPECT), magnetic resonance imaging (MRI), computed tomography (CT), and ultrasound (US) imaging. The higher sensitivity of PET and SPECT than the traditional imaging methods such as MRI, CT, and US has attracted more and more research interests on developing nuclear imaging agents for melanoma detection.[5] Especially, $^{18}$F-Fluoro-deoxyglucose ($^{18}$F-FDG) has demonstrated much higher sensitivity and specificity than those obtained by CT, ultrasound, radiography, and liver function tests and histology or clinical follow-up.[6] Furthermore, $^{18}$F-FDG PET was shown to detect malignant melanoma up to 6 months earlier than those conventional techniques.[7–8] However, because the uptake and cellular retention of $^{18}$F-FDG involve increased glucose metabolism, which also occurs in many other tumor types, or in surgical wounds, pneumonia, and infection/inflammation conditions, $^{18}$F-FDG thus lacks high specificity for melanoma imaging, and false-positive detections often happen.[6–7, 9]

Nuclear imaging modality (SPECT and PET) heavily rely on probes for monitoring specific molecular targets or pathways *in vivo*. Nuclear probes with high specificity based on different targeting or molecular recognition mechanisms help to increase the effectiveness of PET or SPECT for melanoma detection. Therefore, many radiolabeled probes for imaging different molecular targets or processes associated with malignant melanoma have been designed and evaluated for melanoma imaging, such as monoclonal antibodies against melanoma-associated antigens,[10–11] iodoamphetamine,[12] α-melanocyte–stimulating hormone peptides,[13–17] benzamide (BZA)-based compounds.[18–20] So far, BZA analogs have been shown to be among the most promising melanoma targeting agents for both diagnosis and therapeutic applications. *In vitro* cell study demonstrates the high binding affinity of BZA analogs to melanin that presents in melanoma.[21] Moreover, a clinical study using $^{123}$I-labeled BZA for detecting malignant melanoma and its metastases revealed 81% diagnostic sensitivity, 87% accuracy, and 100% specificity.[22] Consequently, the $^{18}$F-labeled BZA ($^{18}$F-FBZA, Figure 1D) has been developed for PET imaging of melanoma and its metastasis using mice bearing B16F10 melanoma tumors.[23–24] It was reported that the B16F10 tumor uptake at 2 h post injection (p.i.) reached 5.94 ± 1.83 percentage injected dose per gram (%ID/g).[23] However, the multistep radiosynthesis of $^{18}$F-FBZA could be a bottleneck for its large production and potential clinical translation.

Recently the pyridine-based precursor, $^{18}$F-6-fluoro-*N*-[2-(diethylamino)ethyl] pyridine-3-carboxamide ($^{18}$F-MEL050, Figure 1C), was successfully synthesized in single step with high radiochemical yield (RCY). This novel PET probe displays excellent performance for imaging of primary and metastatic melanoma.[25–27] In pigmented melanoma B16-F0 xenografts, $^{18}$F-MEL050 exhibits high tumor uptake and tumor-to-background ratio of approximately 50:1 at 2 h p.i. of the probe. The excellent *in vivo* performance of $^{18}$F-MEL050, plus its easy radiosynthesis, encouraged us to design and biologically evaluate more $^{18}$F-MEL050 analogs for melanoma imaging. More specifically, *N*-(2-(diethylamino)ethyl)-$^{18}$F-4-fluoropicolinamide (shortened as $^{18}$F-1**,** Figure 1A), and *N*-(2-(diethylamino)ethyl)-$^{18}$F-5-fluoropicolinamide (shortened as $^{18}$F-2, Figure 1B) were synthesized and side-by-side compared with $^{18}$F-MEL050 (shorted as $^{18}$F-3,, Figure 1C) by small animal PET imaging and biodistribution studies in B16F10-tumor bearing mice.

## Results

### Chemistry and Radiochemistry

The authentic $^{19}$F-fluorine compounds ($^{19}$F-1, $^{19}$F-2, and $^{19}$F-3), and their precursors (**4**, **5**, and **6**, Scheme 1) for $^{18}$F-fluorination were prepared by condensation of a bromopicolinic

acid or bromoniconitic acid with *N,N*-diethylethylenediamine (DEED) *via O*-(*N*-succinimidyl)-1,1,3,3-tetramethyl-uronium tetrafluoroborate (TSTU) activation in the presence of diisopropylethylamine (DIPEA) (Scheme 1 and Supplemental Data). The azeotropically dried $^{18}$F-fluoride can replace the bromo leaving group in each precursor to make the corresponding product in one step. Hence, all of the $^{18}$F-labeled products were prepared within 1 h, including reversed phase high performance liquid chromatography (RP-HPLC) purification and product formulation for further biological evaluation. The resultant products, $^{18}$F-1**,** $^{18}$F-2**,** and $^{18}$F-3, were prepared in radiochemical yields of 24.5 ± 6.7%, 9.5 ± 1.9%, and 21.5 ± 15.5% (n = 3, non-decay corrected), respectively. All the $^{18}$F probes were produced in more than 95% radiochemical purity and free of the corresponding bromo-precursors, as demonstrated by quality control analysis (RP-HPLC). The specific activity for these PET probes was in the range of 100–150 GBq/μmol.

### Small Animal PET Imaging Studies

The tumor-targeting efficacy and imaging property of $^{18}$F-1 and $^{18}$F-2 were evaluated in B16F10 tumor-bearing mice and the results were compared with $^{18}$F-3 which was examined in the same tumor model. In static small animal PET scans, representative coronal images of B16F10 tumor bearing mice (n = 4) at different times after intravenous injection of about 3.7 MBq (100 μCi) of $^{18}$F-1, $^{18}$F-2, or $^{18}$F-3 are shown in Figure 2. B16F10 tumors were clearly visualized with high tumor-to-background contrast at all time points from 0.5 to 2 h. The highest uptakes observed in the kidneys at early time points suggested that these PET probes were mainly excreted through the renal system. Quantification analysis of tumors and other major organ activity accumulation in PET images was done by analyzing the regions of interests (ROIs) that circle the entire organ on the coronal images. The tumor uptakes of $^{18}$F-1 were determined to be 9.52 ± 1.27, 8.97 ± 1.76, 9.73 ± 1.41 %ID/g at 0.5, 1, and 2 h. The tumor uptakes of $^{18}$F-3 were determined to be 7.54 ± 1.60, 7.94 ± 0.96, and 8.47 ± 1.35 %ID/g at 0.5, 1, and 2 h. $^{18}$F-1 and $^{18}$F-3 had much lower tumor uptake compared with $^{18}$F-2, which were 12.74 ± 1.70, 16.61 ± 2.60, and 16.87 ± 1.23 %ID/g at 0.5, 1, and 2 h, respectively (Figure 3 A, B, C).

The higher tumor uptake of $^{18}$F-2 encouraged us to perform a 35-min dynamic small animal PET scans for this novel probe (n = 4). As shown in Figure 3 D, $^{18}$F-2 was rapidly cleared from renal system as determined by ROI analysis of the kidneys. At 5 min after tail vein injection of $^{18}$F-2, radioactivity was rapidly accumulated in kidneys (24.91 ± 5.29 %ID/g) and decreased to 9.44 ± 4.04 %ID/g at 35 min p.i. In contrast, tumor uptake reached 5.28 ± 1.54 %ID/g at 5 min p.i. and gradually increased to the highest 10.52 ± 1.29 %ID/g at the end of the 35 min dynamic scan. During the whole dynamic scan frames, low levels of liver and muscle uptakes were observed.

## Biodistribution Studies

We also performed a biodistribution experiment by direct-sampling tumors and tissues of interest. The results are shown in Table 1. The B16F10 tumor uptakes for $^{18}$F-1 were 7.54 ± 1.64 and 8.66 ± 1.42 % ID/g at 1 and 2 h, respectively, while for $^{18}$F-3, they were 9.54 ± 3.44 and 9.29 ± 2.49 %ID/g at 1 and 2 h p.i.. Both $^{18}$F-1 and $^{18}$F-3 have lower uptake than $^{18}$F-2, which were 15.20 ± 3.37 %ID/g and 16.97 ± 3.28 %ID/g at 1 and 2 h p.i. respectively. Of note, because of the high melanin concentration in C57BL/6 mouse eyes, the uptake of eyes remained at high levels for all three probes. Interestingly, the bone uptakes of $^{18}$F-2 (2.40 ± 0.26 and 1.72 ± 0.45 % ID/g at 1 and 2 h, respectively, n = 4) and $^{18}$F-3 (3.48 ± 0.80 and 2.12 ± 0.38 % ID/g at 1 and 2 h, respectively, n = 4) were significantly lower than those of $^{18}$F-1 (11.29 ± 2.88 and 10.27 ± 3.59 % ID/g at 1 and 2 h, respectively, n = 4) ($P < 0.05$), which indicated that $^{18}$F-2 and $^{18}$F-3 have better *in vivo* stability against defluorination. In comparison, $^{18}$F-1 showed significant defluorination *in*

*vivo* as demonstrated by its high bone uptakes. Moreover, because of the rapid clearance of these $^{18}$F labeled picolinamide probes from normal non-targeted organs, most of the tumor-to-normal tissue ratios increase with time. For examples, the tumor to muscle ratio of $^{18}$F-2 was 13.84 ± 2.38 and 36.79 ± 5.21 at 1 and 2 h, respectively; while for $^{18}$F-3, it was 11.24 ± 2.76 and 15.22 ± 3.91 at 1 and 2 h p.i., respectively (Table 1).

## Discussion and Conclusions

$^{18}$F ($t_{1/2}$ = 109.7 min; $\beta^+$, 99%) is an ideal PET radionuclide for labeling biologically active ligands such as small molecules, peptides or small proteins for PET probe development. The success of $^{18}$F-FDG has made PET a powerful tool in cancer diagnosis, patient stratification, and monitoring the treatment monitoring of cancer patients.[28] In the development of melanoma specific-imaging probes other than the generic tumor imaging probes such as $^{18}$F-FDG, $^{123}$I labeled BZA compounds have been evaluated in melanoma patients with 100% specificity.[22] Because of favorable physical properties of $^{18}$F-fluoride, efforts have been made to develop $^{18}$F-labeled BZA ($^{18}$F-FBZA)[23–24] and $^{18}$F-labeled BZA-like $^{18}$F-MEL050 ($^{18}$F-3).[27] It has been found that $^{18}$F-3 offers high tumor uptakes, fast clearance, and low background.[27] The syntheses of $^{18}$F-**3** analogs have been optimized recently, however, in vivo tumor targeting efficacy was not reported therein[29]. To further develop $^{18}$F-3 analogs with better improved *in vivo* performance, we designed and synthesized $^{18}$F-1 and $^{18}$F-2 herein and compared their *in vivo* tumor imaging properties with $^{18}$F-3 in the same B16F10 melanoma model.

The authentic standards (**1**–**3**) and non-radioactive precursors (**4**–**6**) can be readily prepared in high yields from their corresponding acids. The compounds **1**–**6** were fully characterized using nuclear magnetic resonance (NMR) and electrospray ionization mass spectrometry (ESI-MS). The direct and single step $^{18}$F-fluorination of the precursors can be easily accomplished to achieve the targeted PET probes in good radiochemical yields. Because of the low reactivity of the *3*-position, the RCYs of $^{18}$F-2 are lower than the other two radioligands ($P < 0.05$). However, the radiosynthesis of $^{18}$F-2 can still be easily automated for large quantity synthesis (3.7–37GBq) for potential clinical translation, because of the short synthetic time and the straightforward radiochemistry.

As expected, $^{18}$F-1, $^{18}$F-2, and $^{18}$F-3 all exhibit high tumor targeting efficiency, excellent tumor imaging contrasts, and desirable biodistribution patterns (Figure 2, Table 1). Particularly, $^{18}$F-2 shows significantly lower bone uptakes than that of $^{18}$F-1 and $^{18}$F-3 ($P < 0.05$) (Table 1). Because of the high reactivity of 2- and 4-positions of pyridine ring towards the nucleophilic aromatic substitution[30], some weak nucleophiles, such as water, amino acid or proteins, can potentially replace the $^{18}$F in these two positions. On the contrary, the relative low reactivity of 3-position in the pyridine ring increases the relative *in vivo* stability of $^{18}$F-2. It is of note that the bone uptake of $^{18}$F-1 is about 10 times higher than those of $^{18}$F-2 or $^{18}$F-3, which suggests $^{18}$F in the 4-position is very unstable (Table 1).

In our previous study, $^{18}$F-FBZA was developed as a melanin-targeting PET probe with a chemical structure similar to that of $^{18}$F-2.[23] However, $^{18}$F-FBZA has a much lower tumor uptake in the B16F10 melanoma tumors than that of $^{18}$F-2 (5.94 ± 1.83 %ID/g for $^{18}$F-FBZA at 2 h p.i. *vs.* 16.97 ± 3.28 %ID/g for $^{18}$F-2 at 2 h p.i.). Furthermore, a 3-step radiosynthesis of *N*-succinimidyl 4-$^{18}$F fluorobenzoate ($^{18}$F-SFB) is needed before direct coupling of the $^{18}$F-SFB with the amine compound to prepare $^{18}$F-FBZA, thus the total radiosynthesis time is typically more than 3 h, compared with only 1 h for preparation $^{18}$F-1 and $^{18}$F-2. In this study, we also show that $^{18}$F-2 is superior to $^{18}$F-3 in terms of tumor uptake, tumor to normal organ ratios (Table 1), and tumor imaging contrast (Figure 2). Overall, $^{18}$F-2 is demonstrated to be an excellent candidate for translation as a clinical PET

probe for melanoma diagnosis in term of radiosynthesis, tumor targeting efficiency, and *in vivo* stability.

In conclusion, we designed and synthesized two novel PET probes and a reported PET probe for melanoma diagnosis based on the picolinamide structure. The small animal PET and biodistribution studies in murine melanoma xenografts resulted in excellent tumor imaging contrast using all of these probes. Especially $^{18}$F-2 shows high *in vivo* stability and favorable pharmacokinetic properties such as fast clearance from urinal system and almost background level of uptakes for all of the major organs at 2 h. The high selectivity and specificity of $^{18}$F-2, as evidenced by the high tumor-to-non tumor ratios, highlight that $^{18}$F-2 PET has high potential to improve the melanoma detection. All the desirable properties of $^{18}$F-2 warrant large scale production and potential clinical applications of this novel PET probe.

## Experimental sections

### General

All chemicals obtained commercially were of analytic grade and used without further purification. No-carrier-added $^{18}$F-fluoride was obtained from an in-house PETtrace cyclotron (GE Healthcare). Reversed-phase extraction C18 Sep-Pak cartridges were obtained from Waters and were pretreated with ethanol and water before use. The syringe filter and polyethersulfone membranes (pore size, 0.22 μm; diameter, 13 mm) were obtained from Nalge Nunc International. The semipreparative RP-HPLC using a Vydac protein and peptide column (218TP510; 5μm, 250 × 10 mm) was performed on a Dionex 680 chromatography system with a UVD 170U absorbance detector and model 105S single-channel radiation detector (Carroll & Ramsey Associates). The recorded data were processed using Chromeleon version 6.50 software. With a flow rate of 5 mL/min, the mobile phase was changed from 95% solvent A [0.1% trifluoroacetic acid (TFA) in water] and 5% B [0.1% TFA in acetonitrile (MeCN)] (0–2 min) to 35% solvent A and 65% solvent B at 32 min. Analytical RP-HPLC has the same gradient system except that the flow rate was 1 mL/min with a Vydac protein and peptide column (218TP510; 5 μm, 250 × 4.6 mm). The UV absorbance was monitored at 218 nm and the identification of the small molecules was confirmed based on the UV spectrum acquired using a PDA detector. All synthesized compounds All synthesized compounds showed more than 95% purity (RP-HPLC). Small animal PET scans were performed on a microPET R4 rodent model scanner (Concorde Microsystems Inc.). The scanner has a computer-controlled bed and 10.8-cm transaxial and 8-cm axial fields of view (FOVs). It has no septa and operates exclusively in the 3-dimensional (3D) list mode. Animals were placed near the center of the FOV of the scanner, where the highest image resolution and sensitivity are available.

## Chemistry and Radiochemistry

Preparation of $^{19}$F-1, $^{19}$F-2, $^{19}$F-3 and their bromo-precursor **4**, **5**, **6** (Scheme 1 and Supporting Information)

The same protocol was used for preparation of $^{19}$F-1, $^{19}$F-2, and $^{19}$F-3. As an example, $^{19}$F-1 was synthesized as following. To a solution of 4-fluoropicolinica acid (5.0 mg, 35.5 μmol) in 200 μL of *N,N*-dimethylformamide (DMF) was added TSTU (10.0 mg, 33.0 μmol) and 20 μL of DIPEA. After incubating at 60 °C for 3 h, the reaction mixture was cooled down to room temperature, followed by addition of *N, N*-diethylethylenediamine (7.0 mg, 60 μmol). After 2 h, the mixture was diluted with 1 mL 5% acetic acid solution. The product $^{19}$F-1 was isolated by semi-preparative RP-HPLC. The collected fractions were

combined and acetonitrile was removed under reduced pressure. The final product was obtained by lyophilization.

### *N*-(2-(diethylamino)ethyl)-4-fluoropicolinamide ($^{19}$F-1)

The product was obtained as white powder in the yield of 56% and with 98% purity as determined by RP-HPLC. ESI-MS: m/z 240.3 $[M+H]^+$ ($C_{12}H_{19}FN_3O$, calculated molecular weight: 240.2); $^1$H NMR ($CDCl_3$, 300 MHz): δ = 8.94 (br, 1H), 8.57 (dd, *J* = 5.2 Hz, 9.0 Hz, 1H), 7.83 (dd, *J* = 2.4 Hz, 9.0 Hz, 1H), 7.15 (dd, *J* = 2.4 Hz, 5.2 Hz, 1H), 3.93 (t, *J* = 6.1 Hz, 2H), 3.29 (t, *J* = 5.9 Hz, 2H), 3.22 (q, *J* = 8.6 Hz, 4H), 1.37 (t, *J* = 7.1 Hz, 6H). $^{13}$C NMR ($CDCl_3$, 75 MHz): δ = 167.9, 164.6 (d, $J_{C,F}$ = 101.8 Hz), 152.5, 151.2 (d, $J_{C,F}$ = 6.6 Hz), 114.2 (d, $J_{C,F}$ = 16.5 Hz), 110.4 (d, $J_{C,F}$ = 18.7 Hz), 51.2, 47.3, 35.0, 8.4.

### *N*-(2-(diethylamino)ethyl)-5-fluoropicolinamide ($^{19}$F-2)

The product was obtained as white powder in the yield of 75% and with 98% purity as determined by RP-HPLC. ESI-MS: m/z 240.5 $[M+H]^+$ ($C_{12}H_{19}FN_3O$, calculated molecular weight: 240.2); $^1$H NMR ($CDCl_3$, 300 MHz): δ = 11.35 (br, 1H), 8.41 (d, *J* = 2.7 Hz, 1H), 8.17 (dd, *J* = 4.4, 8.2 Hz, 1H), 7.45 (dd, *J* = 2.7, 8.2 Hz, 1H), 3.88 (t, *J* = 6.1 Hz, 2H), 3.38–3.08 (m, 6H), 1.36 (t, *J* = 7.3 Hz, 6H). $^{13}$C NMR ($CDCl_3$, 75 MHz): δ = 164.9, 161.5 (d, $J_{C,F}$ = 38.5 Hz), 161.4 (d, $J_{C,F}$ = 261.5 Hz), 145.2 (d, $J_{C,F}$ = 4.5 Hz), 137.3 (d, $J_{C,F}$ = 25.4 Hz), 124.0 (d, $J_{C,F}$ = 5.4 Hz), 51.5, 47.2, 34.8, 8.3.

### *N*-(2-(diethylamino)ethyl)-6-fluoronicotinamide ($^{19}$F-3)

The product was obtained as white powder in the yield of 62% and with 97% purity as determined by RP-HPLC. ESI-MS: m/z 240.3 $[M+H]^+$ ($C_{12}H_{19}FN_3O$, calculated molecular weight: 240.2); $^1$H NMR ($CDCl_3$, 300 MHz): δ = 11.00 (br, 1H), 8.80 (d, *J* = 1.7 Hz, 1H), 8.33 (dd, *J* = 1.7, 8.5 Hz, 1H), 6.99 (dd, *J* = 1.7, 8.5 Hz, 1H), 3.82 (t, *J* = 3.9 Hz, 2H), 3.37 (t, *J* = 3.9 Hz, 2H), 3.23 (q, *J* = 7.3 Hz, 2H), 1.35 (t, *J* = 7.3 Hz, 6H). $^{13}$C NMR ($CDCl_3$, 75 MHz): δ = 167.0, 164.6 (d, $J_{C,F}$ = 137.4 Hz), 148.7 (d, $J_{C,F}$ = 15.9 Hz), 140.4 (d, $J_{C,F}$ = 9.3 Hz), 127.1 (d, $J_{C,F}$ = 4.4 Hz), 109.5 (d, $J_{C,F}$ = 37.4 Hz), 52.4, 48.6, 35.8, 8.6.

### 4-bromo-*N*-(2-(diethylamino)ethyl)picolinamide (4)

The product was obtained as white powder in the yield of 82% and with 97% purity as determined by RP-HPLC. ESI-MS: m/z 300.4 $[M+H]^+$ ($C_{12}H_{19}BrN_3O$, calculated molecular weight: 300.1). $^1$H NMR ($CDCl_3$, 300 MHz): δ = 8.97 (br, 1H), 8.40 (d, *J* = 5.2 Hz, 1H), 8.28 (d, *J* = 1.7 Hz, 1H), 7.61 (dd, *J* = 1.7, 3.2 Hz, 1H), 3.91 (t, *J* = 3.7 Hz, 2H), 3.39 (t, *J* = 3.7 Hz, 2H), 3.23 (q, *J* = 7.1 Hz, 4H), 1.34 (t, *J* = 7.1 Hz, 6H). $^{13}$C NMR ($CDCl_3$, 75 MHz): δ = 164.5, 150.2, 149.5, 134.3, 129.8, 125.8, 51.2, 47.1, 34.9, 8.3.

### 5-bromo-*N*-(2-(diethylamino)ethyl)picolinamide (5)

The product was obtained as white powder in the yield of 90% and with 98% purity as determined by RP-HPLC. ESI-MS: m/z 300.4 $[M]^+$ ($C_{12}H_{19}BrN_3O$, calculated molecular weight: 300.1). $^1$H NMR ($CDCl_3$, 300 MHz): δ = 8.90 (br, 1H), 8.62 (s, 1H), 8.01–7.95 (m, 1H), 7.61 (dd, *J* = 1.7, 3.2 Hz, 1H), 3.89 (t, *J* = 5.8 Hz, 2H), 3.26 (t, *J* = 5.8 Hz, 2H), 3.25 (q, *J* = 7.3 Hz, 4H), 1.34 (t, *J* = 7.3 Hz, 6H). $^{13}$C NMR ($CDCl_3$, 75 MHz): δ = 165.1, 149.9, 147.4, 140.0, 124.6, 123.5, 51.4, 47.3, 34.8, 8.3.

### 6-bromo-*N*-(2-(diethylamino)ethyl)nicotinamide (6)

The product was obtained as white powder in the yield of 78% and with 97% purity as determined by RP-HPLC. ESI-MS: m/z 300.2 $[M+H]^+$ ($C_{12}H_{19}BrN_3O$, calculated molecular weight: 300.1). $^1$H NMR ($CDCl_3$, 300 MHz): δ = 9.38 (br, 1H), 8.92 (s, 1H), 8.08 (d, *J* = 8.3 Hz, 1H), 7.55 (d, *J* = 8.3 Hz, 1H), 3.84 (m, 2H), 3.34 (m, 2H), 3.21 (m, 4H), 1.35 (t, *J* = 7.1

Hz, 6H). $^{13}$C NMR ($CDCl_3$, 75 MHz): δ = 165.8, 150.1, 145.7, 137.2, 128.0, 123.8, 52.3, 48.6, 35.7, 8.

## Radiochemistry

An aqueous $^{18}$F-fluoride solution (15 – 30 mCi) was added to a 10 mL vial containing anhydrous acetonitrile (1 mL), $K_{2.2.2}$ (15 mg) and $K_2CO_3$ (3 mg). The solvent was evaporated under a stream of argon at 100 °C under vacuum to produce the $K^{18}F$-$K_{2.2.2}$ complex. This azeotropic drying was repeated twice by anhydrous acetonitrile (2 × 1 mL). The bromo-precursor (**3**, **4**, or **5**) (5 mg) was dissolved in anhydrous DMSO (200 μL) and added to the dried $K^{18}F$-$K_{2.2.2}$ complex. The reaction was stirred and heated at 110 °C for 10 min and cooled down to room temperature. The mixture was then diluted with 1 mL of 5% acetic acid solution for RP-HPLC purification. The collected radioactive peak was dried using a rotary evaporator and the radiolabeled products were reconstituted in phosphate buffered saline (PBS, 0.1 M, pH = 7.4) and passed through a 0.22 μm Millipore filter into a sterile vial for *in vitro* and *in vivo* experiments. The radiochemical yields were calculated based on the obtained radioactive product divided by the activity loaded into the reaction vessel.

## Cell Culture

B16F10 cells were cultured in Dulbecco's modified Eagle high-glucose medium (Gibco Life Sciences) supplemented with 10% fetal bovine serum with penicillin and streptomycin. The cells were regularly maintained in a 37 °C, 5% $CO_2$ humidified incubator.

## Animal Biodistribution Studies

Animal procedures were performed according to a protocol approved by the Stanford University Institutional Animal Care and Use Committee. All of the animals were purchased from Charles River Laboratory. Approximately, cultured B16F10 cells ($1.0 \times 10^6$) were suspended in PBS and subcutaneously implanted in the right shoulders of C57BL/6 mice. Tumors were allowed to grown to a size of 0.5 cm (~ 10 day) before use. For biodistribution studies, the tumor bearing mice (n = 4 for each group) were injected with about 3.7 MBq (100 μCi) of $^{18}$F-1, $^{18}$F-2, or $^{18}$F-3, through the tail vein and sacrificed at 1.0, and 2.0 h p.i.. Tumor and normal tissues of interest were removed and weighed, and their radioactivity was measured in a gamma-counter. The radioactivity uptake in the tumor and normal tissues was calculated as % ID/g.

## Small Animal PET Imaging

For dynamic scan, B16F10 tumor–bearing mice (n = 4) were injected via the tail vein with approximately 3.7 MBq (100 μCi) of $^{18}$F-2, and scans (6 × 20 sec, 8 × 60 sec, 10 × 150 sec, total of 24 frames) were started roughly 2.0 min after the injection of the probe and continued for 35 min. For static scans, the mice bearing B16F10 (n = 4 for each probe), tumor xenografts were injected with about 3.7 MBq (100 μCi) of $^{18}$F-1, $^{18}$F-2, or $^{18}$F-3, *via* the tail vein. At 0.5, 1, and 2 h p.i., the mice were anesthetized with isoflurane (5% for induction and 2% for maintenance in 100% $O_2$) using a knock-down box. With the help of a laser beam attached to the scanner, the mice were placed in the prone position and near the center of the field of view of the scanner. The 3-min static scans were then obtained. Images were reconstructed using a 2-dimensional ordered-subsets expectation maximization (OSEM) algorithm. No background correction was performed. ROIs (5 pixels for coronal and transaxial slices) were drawn over the tumor on decay-corrected whole-body coronal images. The maximum counts per pixel per minute were obtained from the ROI and converted to counts per milliliter per minute using a calibration constant. On the basis of the

assumption of a tissue density of 1 g/ml, the ROIs were converted to counts per gram per min. Image ROI-derived %ID/g values were determined by dividing counts per gram per minute by injected dose. No attenuation correction was performed.

## Statistical Analysis

Quantitative data are expressed as mean ± SD. Means were compared using the Student t test. $P$ values of $< 0.05$ were considered statistically significant.

## Supplementary Material

Refer to Web version on PubMed Central for supplementary material.

## Acknowledgments

This work was supported, in part, by the Melanoma Research Alliance, National Cancer Institute (NCI) In Vivo Cellular Molecular Imaging Center (ICMIC) grant P50 CA114747, and the international cooperation projects of the Chinese Ministry of Science and Technology (2009DFB30040). The authors thank the Radiochemistry Facility of Molecular Imaging Program at Stanford for $^{18}$F-fluoride production.

## Abbreviations

| | |
|---|---|
| **PET** | positron emission tomography |
| **BZA** | benzamide |
| **%ID/g** | percentage injected dose per gram |
| **$^{18}$F-1** | *N*-(2-(diethylamino)ethyl)-$^{18}$F-4-fluoropicolinamide |
| **$^{18}$F-2** | *N*-(2-(diethylamino)ethyl)-$^{18}$F-5-fluoropicolinamide |
| **$^{18}$F-3($^{18}$F-MEL050)** | $^{18}$F-6-fluoro-N-[2-(diethylamino)ethyl] pyridine-3-carboxamide |
| **RCYs** | radiochemical yields |

## References

1. Jemal A, Siegel R, Ward E, Murray T, Xu J, Thun MJ. Cancer statistics, 2007. CA Cancer J Clin. 2007; 57:43–66. [PubMed: 17237035]
2. Jemal A, Siegel R, Xu J, Ward E. Cancer statistics, 2010. CA Cancer J Clin. 2010; 60:277–300. [PubMed: 20610543]
3. Belhocine TZ, Scott AM, Even-Sapir E, Urbain JL, Essner R. Role of nuclear medicine in the management of cutaneous malignant melanoma. J Nucl Med. 2006; 47:957–967. [PubMed: 16741305]
4. Prichard RS, Hill AD, Skehan SJ, O'Higgins NJ. Positron emission tomography for staging and management of malignant melanoma. Br J Surg. 2002; 89:389–396. [PubMed: 11952577]
5. Massoud TF, Gambhir SS. Molecular imaging in living subjects: seeing fundamental biological processes in a new light. Genes Dev. 2003; 17:545–580. [PubMed: 12629038]
6. Eigtved A, Andersson AP, Dahlstrom K, Rabol A, Jensen M, Holm S, Sorensen SS, Drzewiecki KT, Hojgaard L, Friberg L. Use of fluorine-18 fluorodeoxyglucose positron emission tomography in the detection of silent metastases from malignant melanoma. European Journal of Nuclear Medicine. 2000; 27:70–75. [PubMed: 10654150]
7. Holder WD Jr, White RL Jr, Zuger JH, Easton EJ Jr, Greene FL. Effectiveness of positron emission tomography for the detection of melanoma metastases. Ann Surg. 1998; 227:764–769. discussion 769–771. [PubMed: 9605668]

8. Schwimmer J, Essner R, Patel A, Jahan SA, Shepherd JE, Park K, Phelps ME, Czernin J, Gambhir SS. A review of the literature for whole-body FDG PET in the management of patients with melanoma. Q J Nucl Med. 2000; 44:153–167. [PubMed: 10967625]
9. Tyler DS, Onaitis M, Kherani A, Hata A, Nicholson E, Keogan M, Fisher S, Coleman E, Seigler HF. Positron emission tomography scanning in malignant melanoma. Cancer. 2000; 89:1019–1025. [PubMed: 10964332]
10. Beatovic S, Obradovic V, Latkovic Z, Jaksic E. Diagnosis and follow up of primary ocular melanoma by radioimmunoscintigraphy. J BUON. 2004; 9:299–302. [PubMed: 17415830]
11. Voss SD, Smith SV, DiBartolo N, McIntosh LJ, Cyr EM, Bonab AA, Dearling JL, Carter EA, Fischman AJ, Treves ST, Gillies SD, Sargeson AM, Huston JS, Packard AB. Positron emission tomography (PET) imaging of neuroblastoma and melanoma with 64Cu-SarAr immunoconjugates. Proc Natl Acad Sci U S A. 2007; 104:17489–17493. [PubMed: 17954911]
12. Kato K, Kubota T, Ikeda M, Tadokoro M, Abe S, Nakano S, Nishino M, Kobayashi H, Ishigaki T. Low efficacy of 18F-FDG PET for detection of uveal malignant melanoma compared with 123I-IMP SPECT. J Nucl Med. 2006; 47:404–409. [PubMed: 16513608]
13. Cheng Z, Xiong Z, Subbarayan M, Chen X, Gambhir SS. 64Cu-labeled alpha-melanocyte-stimulating hormone analog for microPET imaging of melanocortin 1 receptor expression. Bioconjug Chem. 2007; 18:765–772. [PubMed: 17348700]
14. Cheng Z, Zhang L, Graves E, Xiong Z, Dandekar M, Chen X, Gambhir SS. Small-animal PET of melanocortin 1 receptor expression using a 18F-labeled alpha-melanocyte-stimulating hormone analog. J Nucl Med. 2007; 48:987–994. [PubMed: 17504880]
15. Miao Y, Benwell K, Quinn TP. 99mTc- and 111In-labeled alpha-melanocyte-stimulating hormone peptides as imaging probes for primary and pulmonary metastatic melanoma detection. J Nucl Med. 2007; 48:73–80. [PubMed: 17204701]
16. Ren G, Liu Z, Miao Z, Liu H, Subbarayan M, Chin FT, Zhang L, Gambhir SS, Cheng Z. PET of malignant melanoma using 18F-labeled metallopeptides. J Nucl Med. 2009; 50:1865–1872. [PubMed: 19837749]
17. Ren G, Liu S, Liu H, Miao Z, Cheng Z. Radiofluorinated rhenium cyclized alpha-MSH analogues for PET imaging of melanocortin receptor 1. Bioconjug Chem. 2010; 21:2355–2360. [PubMed: 21073170]
18. Larisch R, Schulte KW, Vosberg H, Ruzicka T, Muller-Gartner HW. Differential accumulation of iodine-123-iodobenzamide in melanotic and amelanotic melanoma metastases in vivo. J Nucl Med. 1998; 39:996–1001. [PubMed: 9627332]
19. Chezal JM, Papon J, Labarre P, Lartigue C, Galmier MJ, Decombat C, Chavignon O, Maublant J, Teulade JC, Madelmont JC, Moins N. Evaluation of radiolabeled (hetero)aromatic analogues of N-(2-diethylaminoethyl)-4-iodobenzamide for imaging and targeted radionuclide therapy of melanoma. J Med Chem. 2008; 51:3133–3144. [PubMed: 18481842]
20. Pham TQ, Berghofer P, Liu X, Greguric I, Dikic B, Ballantyne P, Mattner F, Nguyen V, Loc'h C, Katsifis A. Preparation and biologic evaluation of a novel radioiodinated benzylpiperazine, 123I-MEL037, for malignant melanoma. J Nucl Med. 2007; 48:1348–1356. [PubMed: 17631542]
21. Eisenhut M, Hull WE, Mohammed A, Mier W, Lay D, Just W, Gorgas K, Lehmann WD, Haberkorn U. Radioiodinated N-(2-diethylaminoethyl)benzamide derivatives with high melanoma uptake: structure-affinity relationships, metabolic fate, and intracellular localization. J Med Chem. 2000; 43:3913–3922. [PubMed: 11052796]
22. Michelot JM, Moreau MF, Veyre AJ, Bonafous JF, Bacin FJ, Madelmont JC, Bussiere F, Souteyrand PA, Mauclaire LP, Chossat FM, et al. Phase II scintigraphic clinical trial of malignant melanoma and metastases with iodine-123-N-(2-diethylaminoethyl 4- iodobenzamide). J Nucl Med. 1993; 34:1260–1266. [PubMed: 8326382]
23. Ren G, Miao Z, Liu H, Jiang L, Limpa-Amara N, Mahmood A, Gambhir SS, Cheng Z. Melanin-targeted preclinical PET imaging of melanoma metastasis. J Nucl Med. 2009; 50:1692–1699. [PubMed: 19759116]
24. Garg S, Kothari K, Thopate SR, Doke AK, Garg PK. Design, synthesis, and preliminary in vitro and in vivo evaluation of N-(2-diethylaminoethyl)-4-[18F]fluorobenzamide ([18F]-DAFBA): a

novel potential PET probe to image melanoma tumors. Bioconjug Chem. 2009; 20:583–590. [PubMed: 19222206]

25. Denoyer D, Labarre P, Papon J, Miot-Noirault E, Galmier MJ, Madelmont JC, Chezal JM, Moins N. Development of a high-performance liquid chromatographic method for the determination of a new potent radioiodinated melanoma imaging and therapeutic agent. J Chromatogr B Analyt Technol Biomed Life Sci. 2008; 875:411–418.
26. Greguric I, Taylor SR, Denoyer D, Ballantyne P, Berghofer P, Roselt P, Pham TQ, Mattner F, Bourdier T, Neels OC, Dorow DS, Loc'h C, Hicks RJ, Katsifis A. Discovery of [18F]N-(2-(diethylamino)ethyl)-6-fluoronicotinamide: a melanoma positron emission tomography imaging radiotracer with high tumor to body contrast ratio and rapid renal clearance. J Med Chem. 2009; 52:5299–5302. [PubMed: 19691348]
27. Denoyer D, Greguric I, Roselt P, Neels OC, Aide N, Taylor SR, Katsifis A, Dorow DS, Hicks RJ. High-contrast PET of melanoma using (18)F-MEL050, a selective probe for melanin with predominantly renal clearance. J Nucl Med. 2010; 51:441–447. [PubMed: 20150254]
28. Allen-Auerbach M, Weber WA. Measuring response with FDG-PET: methodological aspects. Oncologist. 2009; 14:369–377. [PubMed: 19357228]
29. Al Jammaz I, Al-Otaibi B, Okarvi S, Amartey J. Rapid and efficient synthesis of [F-18]fluoronicotinamides, [F-18]fluoroisonicotinamides and [F-18]fluorobenzamides as potential pet radiopharmaceuticals for melanoma imaging. Journal of Labelled Compounds & Radiopharmaceuticals. 2011; 54:312–317.
30. Cherng YH. Synthesis of substituted pyridines by the reactions of halopyridines with sulfur, oxygen and carbon nucleophiles under focused microwave irradiation. Tetrahedron. 2002; 58:4931–4935.

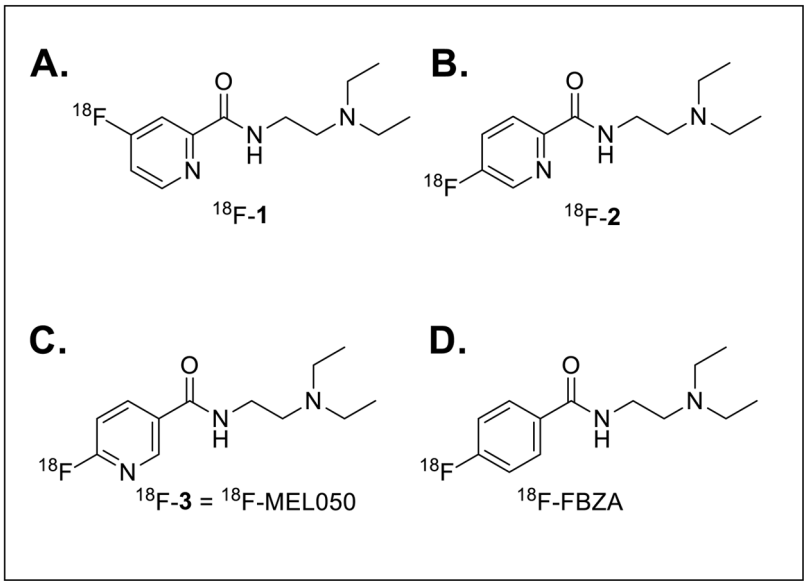


**Figure 1.**
The chemical structures of $^{18}$F-1, $^{18}$F-2, $^{18}$F-3 ($^{18}$F-MEL050) and $^{18}$F-FBZA.

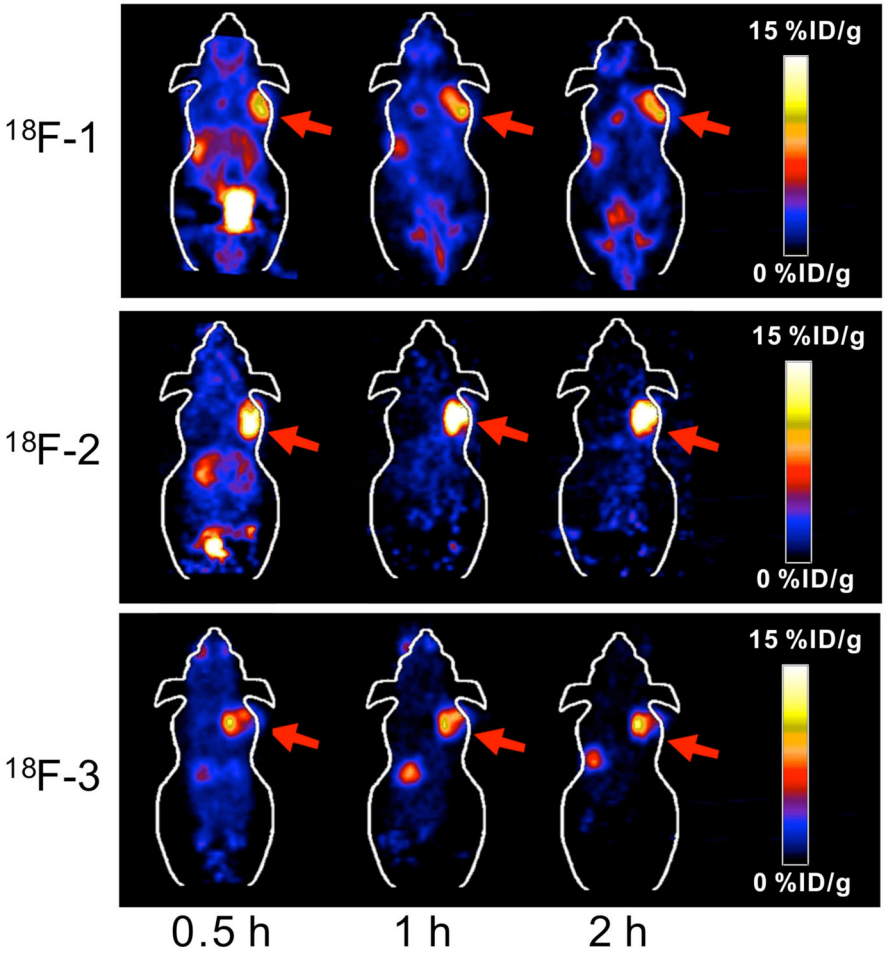


**Figure 2.**
Decay-corrected whole-body coronal small animal PET images of C57BL/6 mice bearing B16F10 murine melanomas from a static scan at 0.5, 1, and 2 h after injection of $^{18}$F-1, $^{18}$F-2, and $^{18}$F-3. Tumors are indicated by arrows.

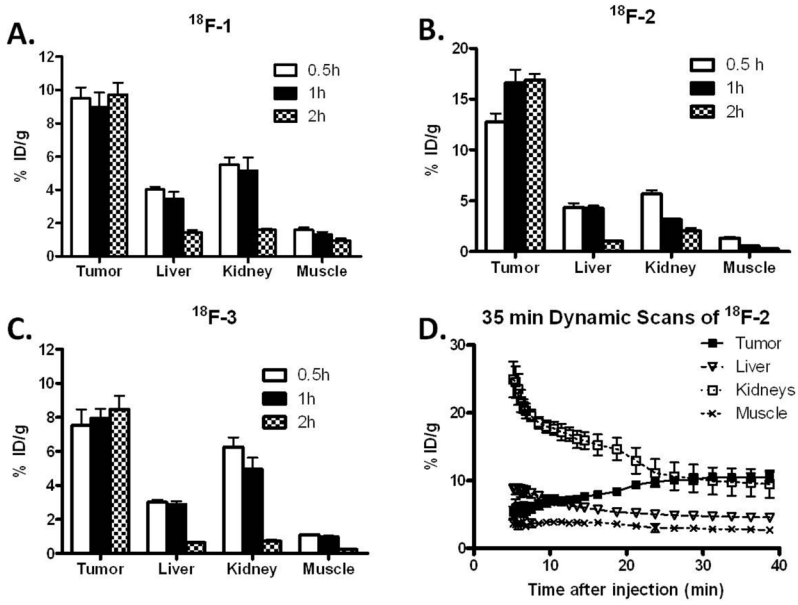


**Figure 3.**

**A, B, C** Small animal PET images quantification of tumors and major organs at 0.5 h, 1 h, and 2 h after injection of $^{18}$F-1, $^{18}$F-2, and $^{18}$F-3 respectively (~100 μCi/mouse, n = 4). **D.** Time–activity curves of tumor and major organs of C57BL/6 mice bearing B16F10 murine melanoma tumors from 35 min dynamic scans after intravenous injection of $^{18}$F-2 (~100 μCi/mouse, n = 4).

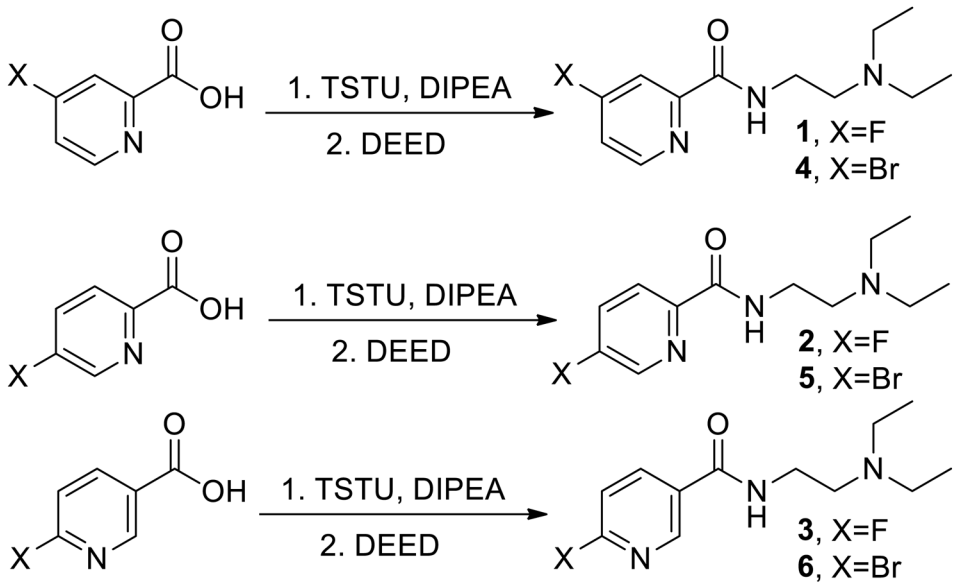


**Scheme 1.**
Synthetic schemes for preparation of the precursors for $^{18}$F-fluorination and $^{19}$F authentic standards.

*J Med Chem*. Author manuscript; available in PMC 2014 February 14.

**Table 1**

Biodistributions of $^{18}$F-1, $^{18}$F-2, and $^{18}$F-3 in C57BL/6 mice bearing B16F10 murine melanoma tumors at 1 and 2 h p.i. Data are expressed as normalized accumulation of activity in %ID/g ± SD (n = 4).

| | $^{18}$F-1 | | $^{18}$F-2 | | $^{18}$F-3 | |
|---|---|---|---|---|---|---|
| **Organ** | **1 h** | **2 h** | **1 h** | **2 h** | **1 h** | **2 h** |
| Tumor | 7.54 ± 1.64 * | 8.66 ± 1.42 * | 15.20 ± 3.37 *† | 16.97 ± 3.28 *† | 9.54 ± 3.44 † | 9.29 ± 2.49 † |
| Blood | 0.33 ± 0.08 | 0.15 ± 0.01 * | 0.42 ± 0.13 | 0.19 ± 0.02 * | 0.46 ± 0.07 | 0.20 ± 0.01 |
| Heart | 0.60 ± 0.07 * | 0.37 ± 0.04 * | 1.17 ± 0.26 * | 0.59 ± 0.04 *† | 1.54 ± 0.53 | 0.40 ± 0.06 † |
| Lungs | 0.88 ± 0.13 * | 0.59 ± 0.08 | 1.58 ± 0.33 * | 0.69 ± 0.07 † | 1.52 ± 0.43 | 0.92 ± 0.13 † |
| Liver | 2.07 ± 0.47 * | 1.41 ± 0.12 * | 4.71 ± 1.47 * | 3.32 ± 0.39 *† | 4.47 ± 2.27 | 1.07 ± 0.25 † |
| Spleen | 1.09 ± 0.87 | 0.31 ± 0.02 | 1.78 ± 0.49 | 1.13 ± 0.87 | 2.88 ± 1.63 | 0.56 ± 0.06 |
| Pancreas | 1.06 ± 0.36 | 0.44 ± 0.02 * | 1.61 ± 0.48 | 0.61 ± 0.04 * | 3.58 ± 1.69 | 0.71 ± 0.07 |
| Stomach | 2.24 ± 0.60 | 1.64 ± 0.59 | 4.26 ± 2.62 | 1.47 ± 0.53 | 5.03 ± 1.78 | 2.27 ± 0.33 |
| Brain | 0.49 ± 0.14 * | 0.24 ± 0.03 * | 1.28 ± 0.33 * | 0.42 ± 0.06 * | 1.56 ± 0.41 | 0.41 ± 0.07 |
| Intestine | 2.28 ± 0.36 | 0.98 ± 0.04 | 2.01 ± 0.47 | 0.88 ± 0.21 | 3.46 ± 1.26 | 0.89 ± 0.53 |
| Kidneys | 1.34 ± 0.28 | 0.69 ± 0.06 * | 3.32 ± 1.23 | 1.03 ± 0.09 * | 5.63 ± 1.72 | 1.20 ± 0.29 |
| Skin | 0.73 ± 0.16 * | 0.63 ± 0.35 | 1.30 ± 0.48 * | 0.68 ± 0.41 | 2.37 ± 0.64 | 0.71 ± 0.39 |
| Muscle | 0.60 ± 0.14 * | 0.20 ± 0.03 | 1.16 ± 0.29 * | 0.41 ± 0.04 * | 1.11 ± 0.18 | 0.52 ± 0.08 |
| Bone | 11.29 ± 2.88 * | 10.27 ± 3.59 * | 2.40 ± 0.26 * | 1.72 ± 0.45 * | 3.48 ± 0.80 | 2.12 ± 0.38 |
| Eyes | 35.96 ± 12.17 | 32.45 ± 3.67 | 37.47 ± 2.55 | 32.83 ± 5.25 | 34.00 ± 9.19 | 32.23 ± 7.73 |
| Uptake Ratio | | | | | | |

| | $^{18}$F-1 | | $^{18}$F-2 | | $^{18}$F-3 | |
|---|---|---|---|---|---|---|
| **Organ** | **1 h** | **2 h** | **1 h** | **2 h** | **1 h** | **2 h** |
| Tumor to Blood | 28.32 ± 3.32 * | 44.33 ± 7.35 * | 41.44 ± 8.09 *† | 88.25 ± 9.77 *† | 20.44 ± 4.34 † | 39.20 ± 4.66 † |
| Tumor to Lung | 8.81 ± 2.44 | 9.46 ± 1.76 * | 9.94 ± 1.29 † | 24.92 ± 6.56 *† | 6.23 ± 0.84 † | 10.49 ± 4.33 † |
| Tumor to Liver | 3.85 ± 1.32 | 4.16 ± 1.25 | 3.79 ± 1.41 | 5.14 ± 1.03 | 2.24 ± 0.32 | 7.26 ± 3.33 |
| Tumor to Muscle | 13.12 ± 4.15 | 27.75 ± 4.24 * | 13.84 ± 2.38 | 36.79 ± 5.21 *† | 11.24 ± 2.76 | 15.22 ± 3.91 † |

*$P < 0.05$, comparison of biodistribution between $^{18}$F-1 and $^{18}$F-2.

†$P < 0.05$, comparison of biodistribution between $^{18}$F-2 and $^{18}$F-3.